Journal of Alloys and Compounds 506 (2010) 141–150

Contents lists available at ScienceDirect

Journal of Alloys and Compounds

journal homepage: www.elsevier.com/locate/jallcom

Ferroelectricity in the glassy material of the composition Bi_2O_3–Pb_3O_4–CuO–K_2O

A.A. Bahgat[a,*], B.A.A. Makram[a], E.E. Shaisha[a], M.M. El-Desoky[b]

[a] Department of Physics, Faculty of Science, Al-Azhar University, Nasr City 11884, Cairo, Egypt
[b] Department of Physics, Faculty of Education, Suze Canal University, El-Arish, Egypt

ARTICLE INFO

Article history:
Received 25 May 2010
Received in revised form 17 June 2010
Accepted 24 June 2010

Keywords:
Bi–Pb–Cu glass
Ferroelectricity
Pyroelectricity
Curie temperature
Dc conductivity

ABSTRACT

Glass sample of the composition 31.4 Bi_2O_3–2.33 Pb_3O_4–64.53 CuO–1.74 K_2O in mol% was prepared by the conventional quenching melt technique. The as-quenched single phase glass shows interesting ferroelectric properties which is not known in the field of glass science. If the as-quenched glass is heat treated above the glass transition temperature all signs of ferroelectricity disappears completely. X-ray diffraction and transmission electron microscopy as well as differential thermal analysis were used to recognize the glassy nature of the as-quenched sample. Ac dielectric measurements were performed as a function of temperature and frequency and showing ferroelectric to paraelectric phase transition at Curie's temperature of 540 K. Non-linear polarization as a function of temperature and applied electric field as well as pyroelectricity were also studied. The conduction mechanism was confirmed to obey the adiabatic small polaron hopping (SPH) and was mainly due to electronic transport between Cu ions. The dominant factor determining conductivity was the hopping carrier mobility in this glass. From the best fits, reasonable values of various SPH and VRH parameters are obtained.

1. Introduction

Since the development made by Duwez [1] and the following success on magnetic metallic [2] and oxide glasses [3], it was a challenge to the scientific community to achieve an equivalent achievement in the field of ferroelectric glassy material. This is due to, on one hand, to the novelty of the problem and the opportunity of manufacturing new materials with unusual properties. On the other hand, by the potentiality of their application in science and engineering. However, basically in ferromagnetic glassy material the magnetic moments can interact within a short range to develop spontaneous alignment and the overall interaction shows ferromagnetic properties. On the other hand, this criterion does not apply to ferroelectric interaction, where a long-range electrical dipoles interaction is necessary; such condition is not fulfilled in a glassy network. Along the years major questions stimulating the study of this type of material were considered, firstly: Does the spontaneous ferroelectric state in homogeneous glass materials is possible? Secondly: How disturbance of the long-range, average-range and short-range order in the arrangement of atoms have an influence on the physical properties of this class of materials? It is necessary to emphasize on that; glassy materials are those amorphous materials showing a glass transition temperature T_g with random distribution of atomic arrangement and short-range order, SRO [4].

Lines [5,6] put forward the first microscopic model, describing the possible occurrence of a ferroelectric instability in an insulating glassy matrix. Using the effective-field theory of statistical mechanics which describe the physical mechanism whereby a dielectric instability might be produced in a glass. This possibility of spontaneous dipolar ordering in bulk amorphous materials prepared on the bases of polar dielectrics was theoretically predicted. According to his model, with great probability one could expect a transition to the macroscopic polar state in those amorphous materials that were prepared by rapid melt quenching of many-axes ferroelectrics, having a high value of spontaneous polarization, for example in $PbTiO_3$. Finally it was noted that in view of the presence of the frozen-in dipoles, these dielectrically soft glasses, whether ferroelectric or not, will show a strong dielectric anomaly at the crystallization temperature. This is due to the decreasingly "frozen" character of the local dipoles as the crystallization instability is approached from below. However, till recently there were no experimental works, in which Lines theory would be reliably enough and explicitly confirmed [5–7].

In a more recent papers, Zhang and Widom [8,9] proposed a mean-field theory that predicts ferroelectric phases in dipolar systems that lacked any specific spatial correlations, provided that the density of the particles was above a critical value. They considered an amorphous solid of dipolar hard spheres where the particles

* Corresponding author.
E-mail address: alaabahgat@hotmail.com (A.A. Bahgat).

0925-8388/$ – see front matter © 2010 Elsevier B.V. All rights reserved.
doi:10.1016/j.jallcom.2010.06.161

were free to rotate, but were frozen at random sites. Their prediction of ferroelectric phases in dipolar systems that lack any specific spatial correlations suggests that well-tuned short-range structure may not be necessary for ferroelectric phase formation. However, Ayton et al. [10,11] applied molecular dynamics and Monte Carlo computer simulations predicted that it is possible to have ferroelectric states without fine-tuned positional correlations. It was predicted also that if a ferroelectric phase is to exist in a positionally random system, the long-range spatially independent correlations arising through the reaction field must dominate the short-range position sensitive correlations, which generally act to frustrate ferroelectric order.

Recently in our series of publications [12–14] it was possible for the first time to demonstrate ferroelectricity in a single phase metastable glassy material namely $Bi_{1.8}Pb_{0.3}Sr_2Ca_2Cu_{3-x}K_xO_z$ ($x = 0.1$–0.4) having spontaneous polarized state. In these publications we put forward another hypothesis [12–14]. According to our original assumptions a ferroelectric state in the investigated glassy materials arises during the manufacture of the bulk glassy samples by ultrarapid melt quenching. Therefore, a polar texture is under anisotropic mechanical stresses induced by melt quenching. This stress induced poling process ought to strain which aligns the internal dipoles within the glass network in a long-range interacting manner and causes it to act very similar as in a crystal, even so the atomic arrangement in the glass structure remains random. This stress-strain induced poling cease completely if the glass sample was annealed at or above the glass transition temperature [12–14] where the glass network is completely relaxed and all microstresses are released. As a result of the ultrarapid quenching a displacement of alkaline cations due to induced strain, e.g., K^+ and probably Ca^{2+}, to off center positions within the glassy network would takes place. This behavior will lead to the ferroelectric performance of the studied material. On the basis of the above and according to the microscopic theory of glasses the quenched state of the glass structure cannot be regarded simply as an arbitrary relaxed glassy random state. This state has very special properties because it is produced by a glass forming quench. The state of the glass is in a metastable phase of equilibrium that is produced by the rapid quenching of a liquid, which suppresses single particle rearrangements. We may therefore state that the main restructuring process which creates this state of the glass is a hierarchy of solid-like structural buckling processes controlled by the internal stress fields in the glass [15].

Verification of these results of ferroelectricity in glasses of the same composition were published recently [16–20]. However, according to transmission electrons micrographs, TEM, Mukherjee et al. [16–18] interpreted the confirmed ferroelectricity as due to nanocrystalline clusters 10–50 nm in size [16–18] containing particles of size less than 10 nm precipitated in their own samples. This interpretation was put forward without any definite theoretical or experimental prove that these nanocrystals are the origin of the observed ferroelectricity. According to these studies [16–18] it is interesting to note that the obtained devitrified state do not show any sign of ferroelectricity or superconductivity. However, it may show superconducting properties under special conditions of crystallization [21,22]. Furthermore, by applying Maxwell–Wagner polarization of heterogeneous components [14] on Mukherjee et al. micrograph results [16–18], it was predicted that the observed ferroelectricity is duo to the glassy part of their sample [14]. In other publications by Geridnev and Repnikov [19,20] ferroelectricity was confirmed further in a similar set of samples, $Bi_{1.8}Pb_{0.3}Sr_2Ca_2Cu_{3-x}K_xO_z$ ($x = 0.1$–0.4), by applying nonlinear dielectric measurements. It was revealed that the value of the dielectric constant decreased by a quadratic law as biased dc field strength is increased. Such behavior of the dielectric permittivity under external bias electric field speaks in favor of a dielectric nonlinearity, which can be described in frames of a thermodynamic theory of ferroelectricity [19,20].

On the other hand, the hypothesis put forward by us [12–14] concerning the effect of the residual microstresses as due thermal quashing on the local dipolar ordering was examined and explicitly confirmed on thin Quasi-amorphous films of $BaTiO_3$ [23,24]. Nevertheless, the generation of electric polarization in an insulating crystalline solid by an elastic strain gradient is referred to as the flexoelectric effect [25].

Alternatively, the dc conductivity of transition metal oxide (TMO) glasses has been targeted for extensive studies [18,26–32] because of their interesting semiconducting properties as well as for their probable technological applications. The conduction mechanism in these glasses was understood by the small polaron hopping (SPH) model [33–35] based on strong electron–lattice interaction. The experimental results of conductivity and other transport properties of many borate glasses containing transition metal ions supported the SPH model [31–36]. At low or intermediate temperatures (below $\theta_D/2$, θ_D: the Debye temperature) where polaron binding energy is less than kT (k is the Boltzmann constant and T is the absolute temperature), the three-dimensional (3D) variable-range hopping (VRH) [33,36] with $T^{1/4}$ dependence of conductivity σ takes place. The VRH was reported for V_2O_5–NiO–TeO_2 [25] and V_2O_5–BaO–B_2O_3 glasses [30]. VRH was reported in BaO–CaO–Fe_2O_3–P_2O_5 glasses [31] as well. However, we reported recently the nature of polaron hopping mechanism (adiabatic or non-adiabatic) in a series of glasses and glass–ceramic nanocrystals of V_2O_5–$BaTiO_3$ series [37]. It should be mentioned that the above two models were based, in common, on a single phonon approach.

In the present work the electrical and ferroelectric properties of a single phase glass sample with the composition 31.4 Bi_2O_3–2.33 Pb_3O_4–64.53 CuO–1.74 K_2O in mol% is examined with the least number of chemical components and showing the ferroelectric properties.

2. Experimental

In the present work a glass sample of the compositions 31.4 Bi_2O_3–2.33 Pb_3O_4–64.53 CuO–1.74 K_2O in mol.% was prepared by the quenched melt technique from reagent grade Bi_2O_3, Pb_3O_4, CuO and K_2CO_3, respectively. The batch was mixed and melted in a platinum crucible at 1000–1050 °C for 30 min during which the melt was stirred to improve the homogeneity. Further increase of the melting temperature above 1050 °C may cause a loss of Bi_2O_3 as due to volatilization. The melt was then poured and rapidly quenched between two copper plates; hammer and anvil. Sheets of opaque black glass samples of 0.5 mm thick were obtained. X-ray diffraction, transmission electron microscopy (TEM) and differential thermal analysis (DTA) were applied to identify the glassy nature of the sample. Dielectric constant, dc and ac electrical conductivity, polarization (P), hysteresis loops ($E-P$) and pyroelectricity measurements were used to identify the electrical properties of the sample as a function of frequency and temperature.

Grounded powder of the as-quenched glass sample was examined by X-ray powder diffraction (XRD) using Cu Kα radiation. Optical microscopy of the polished surface of the sample as well as TEM, using a JOEL-JEM-1010 transmission electron microscope (600,000×) were used to examine the glass sample for possible crystallization. Dc electrical conductivity, σ_{dc}, was measured by the two probe technique as well. Silver painted electrodes were pasted on the two faces of a polished sample. On the other hand, real ε' and imaginary ε'' components of the dielectric constant were performed in the frequency range 0.12–100 kHz and in the temperature range 300–700 K. The ac measurements were obtained using CRL Bridge, Stanford Res. Model SR-720 which is computer controlled. On the other hand the dc conductivity was measured with the aid of HP-425A electrometer. The sample temperature was measured by a chromal–alumal type K thermocouple which is placed as close as possible to the sample. Ferroelectric hysteresis loops were observed using a Sawyer–Tower circuit at temperatures up to 600 K and at a frequency of 70 Hz. The same circuit was used as well for the measurement of the temperature dependence of the polarization over the temperature range 300–600 K. In all these experiments the heating rate was 2 K/min. The polarization as a function of electric field ($E-P$) characteristic was measured at room temperature under ac electric field of frequency 70 Hz with amplitude reaching 15 kV/cm. Pyroelectric current was measured on a previously poled sample (24 V) which was cooled from 570 K to room temperature. The specimen was heated again from room temperature up to 570 K

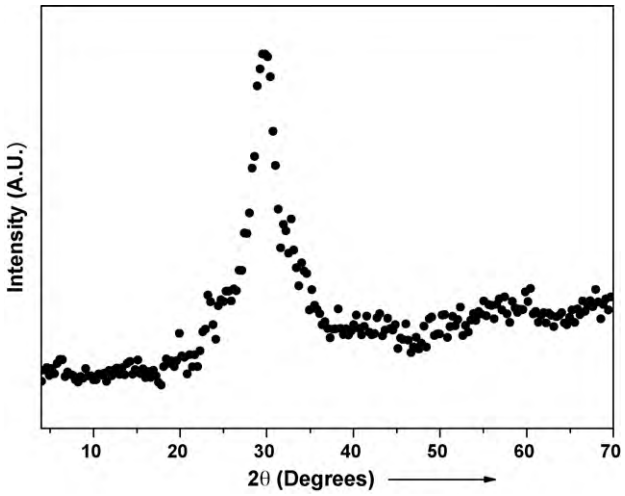

Fig. 1. X-ray diffraction pattern of the glassy material of the compositions 31.4 Bi_2O_3–2.33 Pb_3O_4–64.53 CuO–1.74 K_2O in mol%.

Fig. 3. Electron diffraction micrograph obtained for the as-quenched glass of the compositions 31.4 Bi_2O_3–2.33 Pb_3O_4–64.53 CuO–1.74 K_2O in mol%.

and the pyro-current was monitored by means of a sensitive spot galvanometer, 10^{-9} Amp sensitivity.

3. Results and discussion

3.1. Structural properties

Fig. 1 shows the X-ray diffraction of the as-quenched glass sample. It can be seen that there are only the broad diffraction peak characteristic of glassy structure. Similar patterns were obtained for glasses of comparable constituents [12,22,38]. On the other hand, a TEM micrograph is shown in Fig. 2a and b. It is seen that there is no crystalline precipitation and shows a homogenous glassy state indicating the glassy nature of the samples. In particular Fig. 2b with 500 nm scale a rough surface morphology is observed. Also, by means of the electron diffraction pattern of Fig. 3 the glassy nature of the sample is confirmed, where only a hollow diffraction pattern is observed. These results are in agreement with those obtained by Bahgat and Kamel [12,13] and Bahgat [14] and in disagreement to that obtained afterward by Mukherjee et al. [16–18] concerning nanocrystalline precipitation.

The glassy state of the as-quenched sample was monitored also on the other hand by DTA as shown in Fig. 4. The sample was heated from room temperature up to 850 °K with a rate of 20 °C/min. The DTA thermogram shows two different endothermic and three exothermic transitions. These endothermic peaks were identified as a glass transition temperature, T_g, and the first peak which is

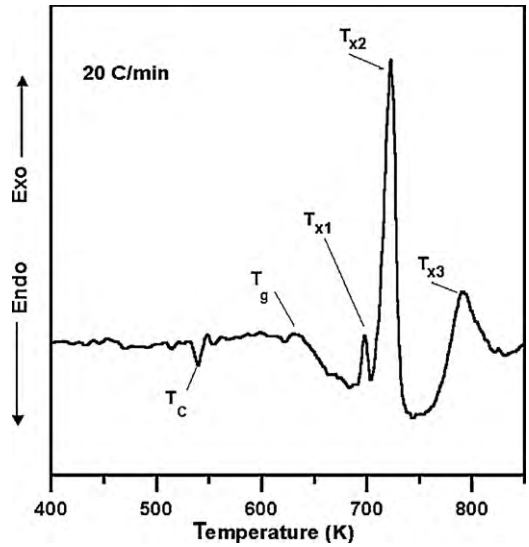

Fig. 4. Differential thermal analysis pattern of the as-quenched glass of the compositions 31.4 Bi_2O_3–2.33 Pb_3O_4–64.53 CuO–1.74 K_2O in mol%, showing the characteristics temperatures; T_C Curie's temperature, T_g glass transition temperature and T_x crystallization temperatures.

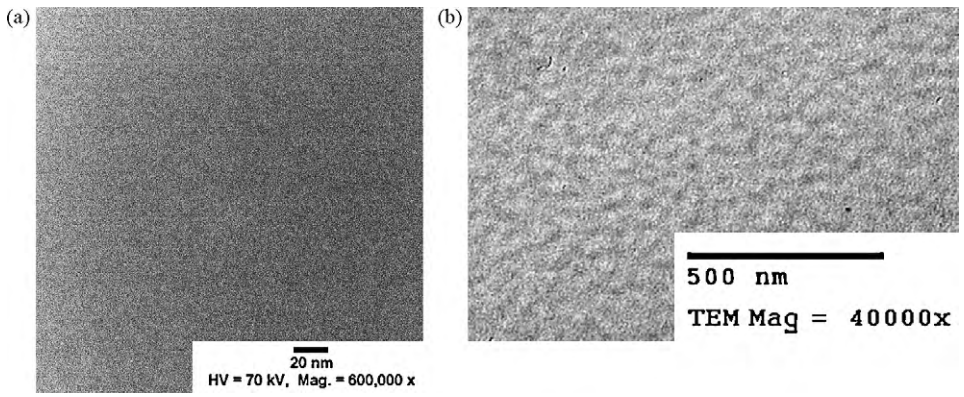

Fig. 2. Typical TEM of the glassy material with the compositions 31.4 Bi_2O_3–2.33 Pb_3O_4–64.53 CuO–1.74 K_2O in mol%.

Table 1
Thermal properties in K.

T_C	T_g	T_{x1}	T_{x2}	T_{x3}	$T_{x1} - T_g$
540	638	690	725	775	84

usually not seen in conventional glasses. This endothermic peak is at a temperature lower than T_g and is designated from the results of the present work as due to a ferroelectric ↔ paraelectric phase transition, i.e. Curie's point T_C. This transition was observed previously for glasses of comparable composition with the addition of CaO and SrO [12–14] and was confirmed by others [16–20] as well. The three exothermic peaks, $T_{x's}$, however, indicate three different crystallization stages of the glass. Table 1 summarizes the results of the DTA measurement. The DTA thermogram shown in Fig. 4 indicate that the endothermic peak at T_C, is due to a first-order phase transition while the sample is remained in its glassy state, where $T_C < T_g < T_x$, as shown. Typically in the field of glass–ceramic ferroelectrics the endothermic peak due to the Curie's temperature is observed in DTA thermograms only after devitrifying the amorphous samples [37,39].

3.2. Ferroelectric properties

3.2.1. Dielectric measurements

Fig. 5 shows the variation of the dielectric constant as a function of temperature at a selected frequency of 0.12 kHz. It can be seen that there are mainly three different maximums. The maximum at 540 K is evidently an indication that the sample is not only in a polar phase but actually it is in a polar glassy phase transition. The fact that DTA data shows an endothermic peak at this same temperature could support the conclusion that our glass sample is actually ferroelectrically ordered below 540 K, namely, the Curie's temperature T_C. While the maximum at 630 K coincide almost with the inflection point of the DTA thermogram (Fig. 4) indicating a glass transition temperature T_g. However, the maximum observed above 670 K is considered as the first crystallization temperature in agreement with the present DTA results shown in Fig. 4. These two successive high temperature peaks, at 630 and 670 K, respectively, may be explained by the two abnormalities predicted by Lines theory [5]. Commonly, at the crystallization temperature (T_{x1} = 690 K) the ions take part in rapid movements to change from a random or glassy to ordered crystalline conditions and hence the higher dielectric constant via higher conduction-related polarization. Further, the dielectric anomaly around the crystallization temperature in glass of the present kind would arise from the anomalies that are likely to take place in the thermodynamic parameters such as specific heat (C_p) and entropy [40]. In addition, the high value of the dielectric constant, 15,000, at the Curie's temperature is common at the transition [41].

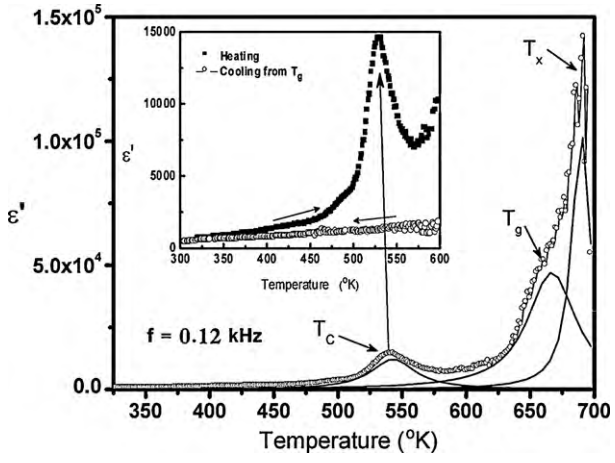

Fig. 5. Dielectric permittivity scan as a function of temperature at applied frequency of 0.12 kHz. The insert shows an enlarged portion of the scan showing the behavior at the Curie's temperature together with the trend as the temperature is lowered from above T_g – open circles "o".

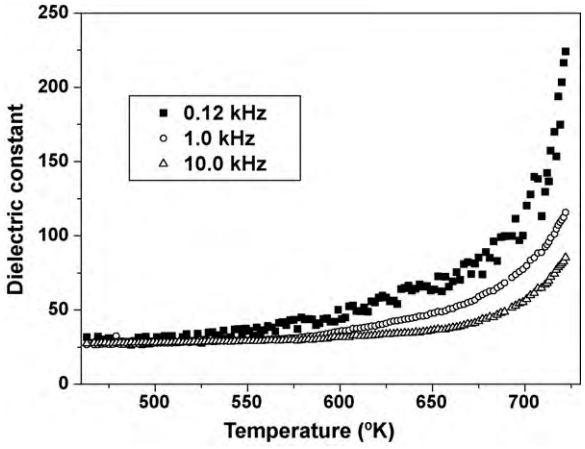

Fig. 6. Representative dielectric permittivity as a function of temperature with different applied frequency of the heat treated glass above T_g, showing no sign of ferroelectric transition at 540 K.

In addition, it is also shown in the insert of Fig. 5 (open circles) that while cooling the glass sample from or above T_g to room temperature the peak at 540 K connected to the Curie's temperature T_C vanishes completely. Whereas if the sample was detached from the oven at a temperature in between T_C and T_g, while a second set of dielectric measurements is done the peak observed at 540 K continue to be present with almost the same high values of permittivity, similar results was reported in our earlier work [14]. This observation may be explained by the knowledge that on annealing a glass at the glass transition temperature all residual microstresses developed in the glass as due to fast quenching are vanished. This test Indicate that the observed ferroelectric instability should have an origin due to the residual microstresses and the associated microstrains developed in the as-cast glass during fast quenching of the melt. In addition, it should be mentioned that if the glass sample was heat treated at or above the crystallization temperatures T_x no indication of ferroelectricity is observed as shown in Fig. 6. During this set of measurements the usual Debye's dielectric behavior is seen [38], together with a tremendous drop in the values of the permittivity are detected.

On the other hand, the dielectric constant data could be treated according to the Curie–Weiss relation [42], the results are presented in Fig. 7 and Table 2:

$$\varepsilon' = \frac{C}{T - T_o} \quad (1)$$

here C is the Curie constant indicating a displacive phase transition [42]. While T_o = 517 K is the extrapolated intersection of the high temperature part of the plot with the temperature axis as shown in Fig. 7. However, to identify the order of this transition it is usually a general practice to find out the ratio, n, of the slopes, $\partial(1/\varepsilon)/\partial T$, below and above T_C, which is ($n = -3.43$), see Fig. 7. This value indicates according to the theory of Devonshire [42] that the observed transition is of first-order type in agreement with the above DTA results and is due to metastability at the transition. It is observed that the Curie constant is in the same order of magnitude of crystalline materials, e.g., $C = 1.8 \times 10^5$ K for $BaTiO_3$ [42].

On the other hand, Fig. 8 shows the variation of the loss in terms of, tan(δ). It is seen that there are two independent loss peaks of the

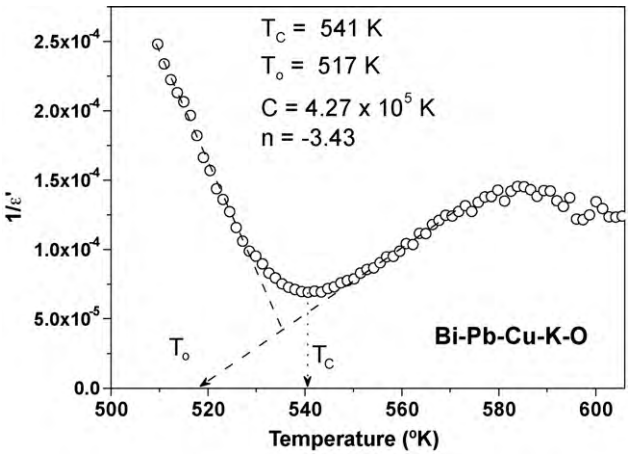

Fig. 7. Application of the Curie–Weiss law of ferroelectricity ($1/\varepsilon'$) as a function of temperature at 0.12 Hz.

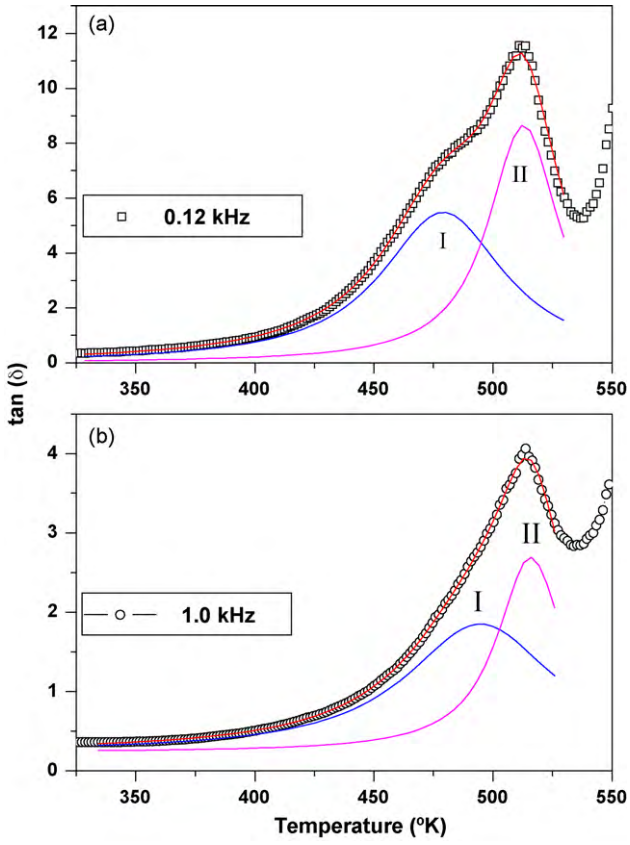

Fig. 8. Representation of the dielectric loss in terms of tan(δ) at two different frequencies (0.12 and 1.0 kHz, respectively), showing the Debye relaxation peak (in blue) and the ferroelectric transition peak (in violet), respectively. (For interpretation of the references to color in this figure legend, the reader is referred to the web version of the article.)

same order of magnitude. It is clear that the low temperature peak, *I*, is shifted to higher temperature as the applied frequency increases indicating a Debye type relaxation [38,43]. Nevertheless, the temperature position of the second high temperature peak, II, was not

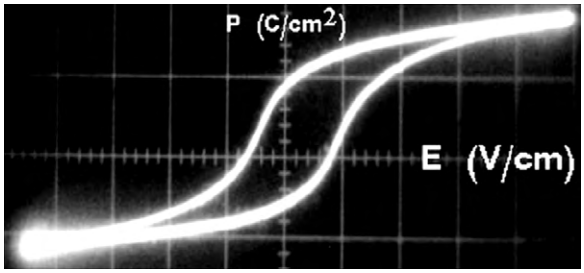

Plate 1. 70 Hz and 12 kV/cm electric field hysteresis loop recorded at room temperature of the as-quenched glass of the compositions 31.4 Bi_2O_3–2.33 Pb_3O_4–64.53 CuO–1.74 K_2O in mol%.

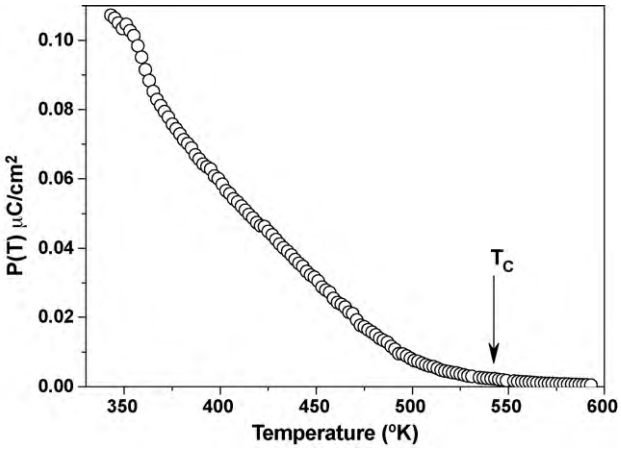

Fig. 9. Representation of the electric polarization as a function of temperature at 70 Hz excitation showing the Curie's temperature T_C.

affected by altering the applied frequency indicating a ferroelectric transition [13] as shown in Fig. 8b. Generally, the dielectric loss factor tan(δ) follows temperature behavior similar to that of the dielectric constant ε_r [42]. If the phase transition is sharp, ε_r and tan(δ) peaks at the same temperatures and both follow Curie–Wiess law as expected from Kramrs–Kroning relations [42]. However, if the phase transition is not well defined, then ε_r and tan(δ) peaks at different temperatures with $T_C(\tan(\delta)) < T_C(\varepsilon_r)$, as in the present work. Commonly the temperature separation of the two maxima depends on the degree of disordering of the material structure and on the temperature dependence of the dielectric relaxation.

3.2.2. Non-linear polarization and hysteresis loop

Generally, ferroelectricity is a spontaneous electric polarization of a material that can be reversed by the application of an external electric field. In addition a common requirement of ferroelectricity is the non-linear rise of polarization, *P*, as a function of applied electric field, *E*, and which can be reversed as well. This to gather with the ability of the ferroelectric material to show a permanent polarization. Such properties may be easily recognized by studding the hysteresis loop. Plate 1 shows a representing example of room temperature hysteresis loop (*E*–*P*). The loop proves the ferroelectricity nature of the present as-quenched amorphous sample. On the other hand, Fig. 9 describes the non-linear behavior of polarization as a function of temperature as extracted from the *E*–*P* hysteresis loops

Table 2
Ferroelectric parameters and spontaneous polarization at room temperature.

T_o (K)	T_C (K)	C (K)	n	T_C (tan (δ)) (K)	ε_r at RT 0.12 kHz	ε_r at *RT* 100 kHz	Polarization ($\mu C/cm^2$)
517	541	$4.27 \times 10^{+5}$	−3.43	512	560	120	0.107

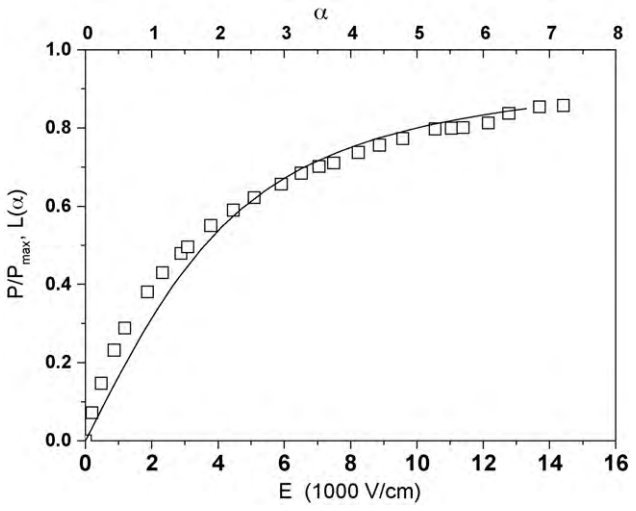

Fig. 10. 70 Hz electric field effect on the polarization of the as-quenched glass of the compositions 31.4 Bi_2O_3–2.33 Pb_3O_4–64.53 CuO–1.74 K_2O in mol%. The solid curve is an application of the Langevin's function Eq. (3).

according to the relation [5]:

$$\frac{P(T)}{P(RT)} = \left[\frac{T_C - T}{T_C}\right]^{1/2} \quad (2)$$

Further verification of the non-linear behavior of the reduced polarization as a function of the applied electric field may be examined by applying the Langevin's function [44]:

$$L(\alpha) = \coth(\alpha) - \frac{1}{\alpha} \quad (3)$$

where $\alpha = pE_l/kT$, E_l is the local electric field, p is the electric dipole moment, k is the Boltzmann constant and $L(\alpha) = P(E)/P_{max}$ at a specific temperature T. It is seen from Fig. 10 that the continuous curve described by Eq. (3) illustrate very well the experimental data. This result shows that this glass sample is a polar material with all the properties of a ferroelectric material unless the temperature did not reach the glass transition temperature T_g. According to the obtained results one may address the studied glass sample as soft ferroelectric.

3.2.3. Pyroelectricity

Generally, it is recognized that all ferroelectric materials should posses both the properties of piezoelectricity as well as pyroelectricity, however the reverse is not essentially applies. Accordingly, the observation of pyroelectricity is necessary but not sufficient to prove the existence of ferroelectricity in a material. Where pyroelectricity is defined as the change of polarization of a dielectric with temperature after eliminating polarization effects produced by thermal strains which accompany the temperature changes, i.e. temperature dependence of the spontaneous polarization in certain anisotropic solids [45]. If such a material is heated the resulting dimensional changes will cause a change in its dipole moment (other factors, such as change of dielectric constant with temperature, may also contribute to this change of dipole moment). Therefore, whenever there is a change of temperature the magnitude of surface charge requires modification to restore electrical equilibrium with the ambient. This adjustment is not immediate, and until it is complete there is an electric potential difference between the ends of the material. Thus an effect of a temperature change upon this type of material is to produce a transient electric potential difference known as "pyroelectric".

The variation of pyroelectric coefficient as a function of temperature for the as-quenched glass is shown in Fig. 11. The results of the measurements of the pyroelectric current and coefficients obey the equation given by [42]:

$$i = A\left(\frac{dP}{dT}\right)\cdot\left(\frac{dT}{dt}\right)$$

where dP/dT is the pyroelectric coefficient evaluated at temperature T and A is the surface area normal to the polar axis. The glass was heated inside the furnace and the pyroelectric current was measured in the temperature range 300–570 K as explained above. The heating rate (dT/dt) was fixed at 2 K/min. Indeed the pyroelectric behavior of the glass is analogous to that of thermal behavior observed in DTA. However, the difference in the temperature of the incidence of this peak at 475 K from that of DTA study is attributed to different time scales. Non-ferroelectric dielectric glasses with pyroelectric properties are familiar in this field [46].

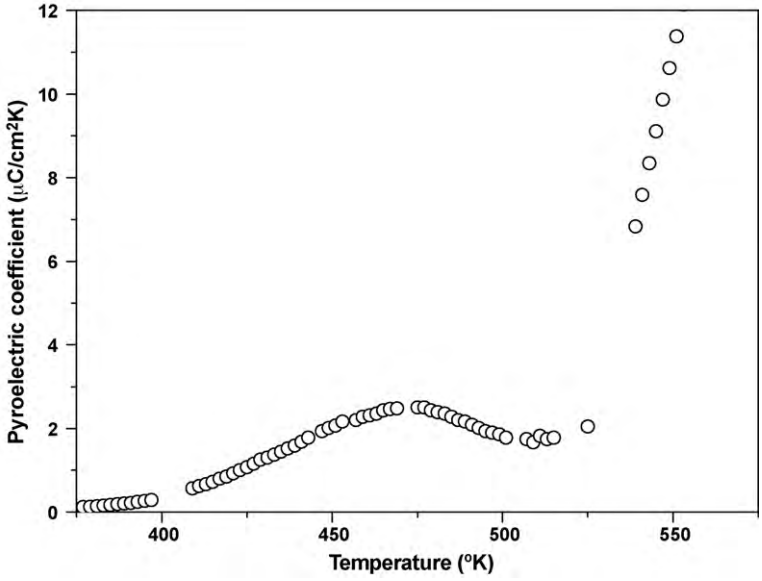

Fig. 11. Pyroelectric coefficient as a function of temperature for the as-quenched glass of the compositions 31.4 Bi_2O_3–2.33 Pb_3O_4–64.53 CuO–1.74 K_2O in mol%.

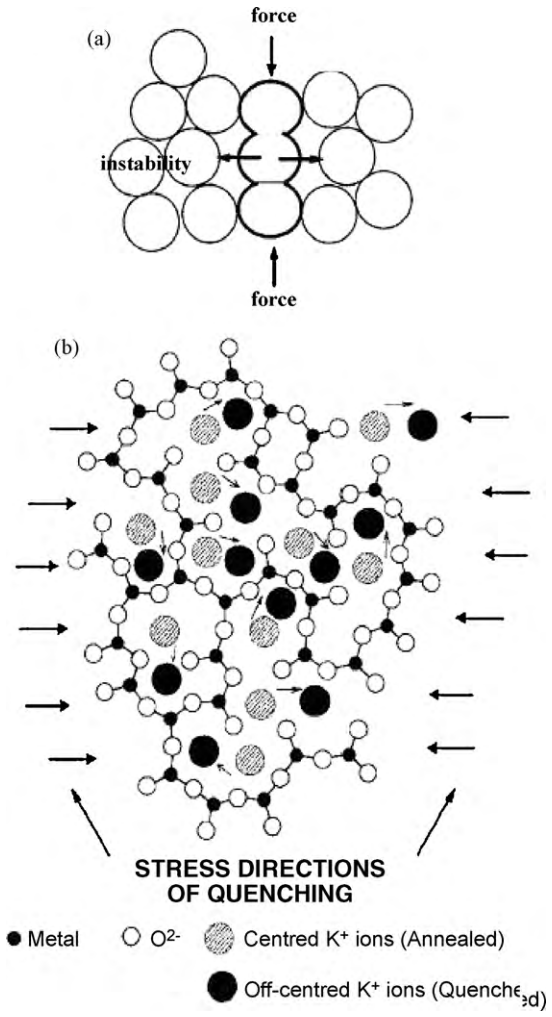

Fig. 12. Proposed two-dimensional simple glass structure during the process of quenching (a) and (b) the detestable frustrated glass structure below the glass transition temperature T_g, showing the off center positions of the alkaline metal [14].

3.3. Structure model

In a glass which has been cooled from the melt without any special treatment the individual dipoles will be randomly oriented and there will in consequence be no total dipole moment. At room temperature the dipoles are not rotatable by an applied electric field because they lie in potential wells having activation energies much larger than kT (the product of Boltzmann's constant with absolute temperature) of room temperature. All glasses show a T_g above which they behave like very viscous liquids. Structural reorientations become possible at or above this temperature. On the other hand, if the glass melt was quenched vigorously, e.g., between two metal blocks, the melt will be frozen rapidly in to a solid glass. This glass would have a very special structure of quite different overall random atomic arrangements with modified potential well different from that which is left to freeze without any special treatment.

Fig. 12a and b, show a two-dimensional simple model scheme predicts a very special state for the glass in which the internal stresses are correlated with the local structure in an important way. This state may create some sort of molecular order along the stress axis, i.e. quenching direction. This also predicts that the quenched state of the glass which creates instabilities is very different from the random medium and in which one can neglect the effect of internal stresses. Further theoretical development of this model is to be published elsewhere. Accordingly, one may assume that the ferroelectricity that was observed in the present work have an origin as due to the residual microstresses developed during the quenching of the glass melt. If the glass transition temperature T_g is reached, those residual microstresses will vanish due to annealing, hence the ferroelectric instability disappears, i.e. in the present case K^+ ions are at center positions and instability is removed, and the ferroelectricity disappears as shown in Figs. 5 and 6.

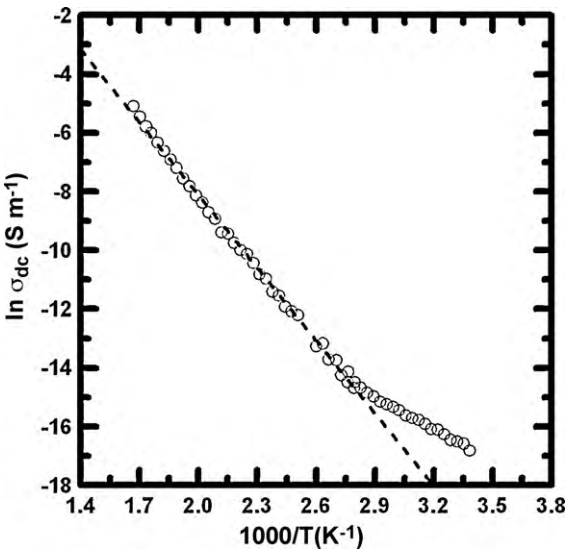

Fig. 13. Direct current electrical conductivity as a function of reciprocal temperature according to Eq. (4), of the as-quenched glass of the compositions 31.4 Bi_2O_3–2.33 Pb_3O_4–64.53 CuO–1.74 K_2O in mol%.

3.4. Dc electrical conductivity

Fig. 13 shows the relation between the dc conductivity σ of the glass and inverse temperature. This glass has σ from 4.14×10^{-8} to 9.59×10^{-3} S m^{-1} at temperatures from 295 to 600 K. Fig. 13 clearly gives the linear relationship between $\ln\sigma$ and T^{-1}. The slope of the curve which gives the activation energy, W, for conduction, however, has two different values and increase towards higher temperatures. For this linear curve with different slopes in the two-temperature regions (295–350 and 350–600 K), σ is expressed as:

$$\sigma = \left(\frac{\sigma_o}{T}\right) \exp\left(\frac{-W}{kT}\right) \quad (4)$$

where σ_o is a re-exponential factor, W is the activation energy and k is the Boltzmann constant.

The logarithm of conductivity (Fig. 13) shows linear – temperature – dependence up to critical temperature $\theta_D/2$ and then the slope changes with deviation from linearity and the activation energy is temperature dependent. Such a behavior was found in $SrTiO_3$–V_2O_3–PbO_2 [26] and V_2O_5–BaO–B_2O_3 glasses [27]. This phenomenon is attributed to the change of conduction mode from SPH to VRH with decrease in temperature [28,29]. We then assumed that changes in the slopes were caused by a transition from SPH to intermediate VRH in the present case [30,31].

Austin and Mott [32] have proposed a model for conduction processes in the transition metal oxide (TMO) glasses. In this model, the conduction process is considered in terms of phonon assisted hopping of small polarons between localized states. The dc conductivity in the Mott model for the nearest neighbor hopping in non-adiabatic regime at high temperatures ($T > \theta_D/2$) is given by

Table 3
Transport properties of Bi_2O_3–Pb_3O_4–CuO–K_2O glass.

Activation energy, W, above 385 K	0.71 (eV)
Density, d	7.08 (g cm^{-3})
Transition metal ion sites per unit volume, N	1.98×10^{22} (cm^{-3})
Hopping distance, R	0.369 (nm)
Polaron radius, r_p	0.148 (nm)
Debye temperature, θ_D	700 (K), 486 (cm^{-1})
Disorder energy, W_D	0.025 (eV)
Polaron hopping energy, W_H	0.135 (eV)
$\Delta W = W - W_H$	0.575 (eV)
Fraction of reduced transition metal ion, $C = Cu^+/Cu_{total}$	0.81
Pre-exponential factor, $\ln\sigma_o$ (S m^{-1})	7.85
Density of state at Fermi level, $N(E_F)$	6.69×10^{21} (eV^{-1} cm^{-3})
Small polaron coupling constant, γ_p	4.4
Effective dielectric constant, ε_p	152
High frequency ε_∞ (100 kHz)	120
Static dielectric constant, ε_s (0.12 kHz)	560
Optical phonon frequency, ν_o	1.48×10^{13} (s^{-1})
Polaron band width, J	0.14 (eV)
Decay constant, α	1.46 (nm^{-1})
Parameter, A	36.95 (S m^{-1} K$^{1/2}$)
Parameter, B	208.72 (K$^{1/4}$)
Hopping carrier mobility (400 K), μ	1.63×10^{-6} (cm^{-2} V^{-1} s^{-1})
Hopping carrier density (400 K), N_c	8.10×10^{19} (cm^{-3})

Eq. (4) while the pre-exponential factor, σ_o, is given by

$$\sigma_o = \frac{\nu_o N e^2 R^2 C(1-C)\ \exp(-2\alpha R)}{k} \tag{5}$$

where ν_o is the optical phonon frequency, C the fraction of reduced transition metal ion ($C = Cu^+/Cu_{total}$), α the tunneling factor [31], N the transition metal ion sites per unit volume and R the hopping distance. The relationship between N and R is generally described as follows:

$$R = \left(\frac{1}{N}\right)^{1/3} \tag{6}$$

The calculated values of R and N are summarized in Table 3.

In the adiabatic hopping regime, however αR in Eq. (5) becomes negligible [33,34], then the conductivity, σ, and the pre-exponential factor σ_o in Eq. (5) is expressed by the following equation [28,29]:

$$\sigma_o = \frac{\nu_o N e^2 R^2 C(1-C)}{k} \tag{7}$$

Assuming a strong electron phonon interaction, Austin and Mott [32] have shown that the activation energy, W, is the result of polaron formation of binding energy, W_p, and an disorder energy, W_D, which might exist between the initial and final sites due to variation in the local arrangements of ions, i.e.:

$$\begin{aligned} W &= \frac{W_H + W_D}{2} \quad \text{for} \quad T > \frac{\theta_D}{2} \\ &= W_D \quad \text{for} \quad T < \frac{\theta_D}{4} \end{aligned} \tag{8}$$

where W_H ($=W_p/2$) is the polaron hopping energy.

Holstein [35] has suggested a method for calculating the polaron hopping energy W_H:

$$W_H = \left(\frac{1}{4N}\right) \sum\nolimits_p [\gamma_p]^2 \hbar\omega_p \tag{9}$$

where $[\gamma_p]^2$ is the electron–phonon coupling constant and ω_q is the frequency of the optical phonons. Bogomolov et al. [36] on the other hand have calculated the polaron radius, r_p, for a non-dispersive system of frequency ν_o in Eq. (7):

$$r_p = \left(\frac{\pi}{6}\right)^{1/3} \frac{R}{2} \tag{10}$$

The value of the polaron radii as calculated from Eq. (10), using R from Table 3 is shown in Table 3 for the present glass. Although the possible effect of disorder has been neglected in the above calculation, the small value of polaron radii suggests that the polarons are highly localized [28,38]. The polaron hopping energy W_H is given by [36]:

$$W_H = \frac{e^2}{4\varepsilon_P}\left(\frac{1}{r_P} - \frac{1}{R}\right) \tag{11}$$

where

$$\frac{1}{\varepsilon_P} = \frac{1}{\varepsilon_\infty} - \frac{1}{\varepsilon_S} \tag{12}$$

ε_s and ε_∞ are the static and high frequencies dielectric constants of the glass, respectively. An estimate of W_H can be made from Eq. (11) from the known values of R and r_p, while ε_∞ was taken at 100 kHz. The values of W_H and ε_P are given in Table 3.

According to Miller and Abrahams [47] the disorder energy defined as the difference of electronic energies between two hopping sites [28,29] and is given by

$$W_D = \left(\frac{e^2}{\varepsilon_S R}\right) l \tag{13}$$

l is a constant of the order 0.3.

The difference existing between W and W_H arises from the disordering term $W_D/2$ and can be calculated from Eq. (8). An evaluation of W_D from Eq. (17) gave $W_D = 0.025$ eV. It is seen from Table 3 that $\Delta W = W - W_H$ (0.575 eV) is higher than the calculated value. Similar results have been reported for other borate and vanadate glasses [29,37,44]. This discrepancy had been explained as the effect of the partial charge of the cations of the glass forming oxides on activation energy for hopping conduction in TMO glasses [29,37,48].

The density of state at Fermi level can be estimated from the following expression [28]:

$$N(E_F) = \frac{3}{4\pi R^3 W} \tag{14}$$

The results for the present glass are listed in Table 3. The value of $N(E_F)$ is reasonable for localized states.

A polaron hopping model has been investigated by Friedman and Holstein [48] considering zero disorder energy and covering both the adiabatic and non-adiabatic hopping processes. On the basis of molecular crystal model, Friedman and Holstein [49] have derived an expression for the dc conductivity of the form:

$$\sigma = \left(\frac{3e^2 N R^2 J^2}{2kT}\right)\left(\frac{\pi}{kTW_H}\right)(-2\alpha R)\exp\left(\frac{-W_H}{kT}\right) \tag{15}$$

for the case of non-adiabatic hopping, while Emin and Holestein [50] have shown that for the case of adiabatic hopping:

$$\sigma = (8\nu_o \pi e^2 N R^2/3kT)\exp\left[\frac{-(WH^{-J})}{kT}\right] \tag{16}$$

where J is a polaron band width related to electron wave function overlap on the adjacent sites. This model provides an independent way of ascertaining the nature of hopping mechanism at high temperatures. The condition for the nature of hopping can be expressed by [50]:

$$J > \left(\frac{2kTW_H}{\pi}\right)^{1/4}\left(\frac{\hbar\nu_o}{\pi}\right)^{1/2} \quad \text{(adiabatic)} \tag{17}$$

and

$$J < \left(\frac{2kTW_H}{\pi}\right)^{1/4}\left(\frac{\hbar\nu_o}{\pi}\right)^{1/2} \quad \text{(non}-\text{adiabatic)} \tag{18}$$

The condition for formation of small polaron is, however, given by $J \leq W_H/3$ [37]. The limiting value of J calculated from the right-hand

side of expression (17) or (18) at 400 K is of the order of 0.013 eV, and therefore the condition for the existence of small polaron is satisfied. An unambiguous decision as to whether the polaron is actually in the adiabatic or in the non-adiabatic regime requires an estimate of the value of J, which can be obtained from [28]:

$$J \approx e^3 \left[\frac{N(E_F)}{(\varepsilon_o \varepsilon_p)^3} \right]^{1/2} \quad (19)$$

Using the values of $N(E_F)$ and ε_p from Table 3, Eq. (19) gives $J \approx 0.14$ eV and thus the adiabatic hopping theory is most appropriate to describe the polaronic conduction at high temperatures in the present glass. Here ε_o is the free space permittivity.

Next, we estimate the optical phonon frequency (ν_o) in Eq. (7) using the experimental data from Table 3, according to $k\theta_D = h\nu_o$ (h is the Plank's constant) [37]. To determine ν_o for the present composition, the Debye temperature θ_D of the present glass was obtained to be 700 K at the inflection point of Fig. 13, which is nearly the same as that of V_2O_5–P_2O_5 [51], alkaline silicate glasses [52] and V_2O_5–$BaTiO_3$ glass [37]. Thus, this estimated θ_D value is physically reasonable. Then, with the θ_D value, ν_o was calculated using $\nu_o = k\theta_D/h$. The values of θ_D and ν_o are summarized in Table 3. Nevertheless, the value of the fraction of reduced transition metal ion ($C = Cu^+/Cu_{total}$) as calculated from Eq. (10), using R, N, ν_o and σ_o from Table 3 is shown in Table 3 for the present glass.

The value of small polaron coupling constant γ_p, which is a measure of electron–phonon interaction, and is given by the formula $\gamma_P = 2W_H/h\nu_o$ [53] was also evaluated for the present glass. The estimated value of γ_p is 4.4 accordingly see Table 3. This value is found smaller than those for V_2O_5–Bi_2O_3 glasses doped with $BaTiO_3$ (7.05–7.60) [54] and larger than those for WO_3–$Na_2B_4O_7$ glasses (0.190–0.359) [55]. The value of γ_p >4 usually indicates a strong electron phonon interaction [56].

The hopping of carriers mobility, μ, and their density, N_c were estimated for the present glass. For adiabatic hopping regime, μ is given by [28]:

$$\mu = \left(\frac{\nu_o e R^2}{kT} \right) e^{-W_H/kT} \quad (20)$$

then, μ value was calculated at $T = 400$ K using the experimental data of ν_o, R and W_H evaluated for present glass. Also N_c value was evaluated using the conductivity formula $\sigma = eN_c\mu$. The values of μ and N_c of the present glass composition are given in Table 3. The mobility at 400 K for present glass is very small (1.63×10^{-6} cm^2 V^{-1} s^{-1}), suggesting that electrons are localized at Cu ions [28,49]. Since the conduction of localization for conductive electrons is generally $\mu < 10^{-2}$ cm^2 V^{-1} s^{-1} [57], the result indicates that electrons in the present glass are localized mainly at Cu ions sites. Further, $N_c \sim 10^{19}$ cm^{-3} indicates that the conductivity of the glass is primarily determined by the hopping mobility [32,58]. Similar results were obtained for $SrTiO_3$–V_2O_3–PbO_2 andV_2O_5–NiO–TeO_2 glasses [26,59].

In Fig. 12 we notice that the temperature dependence of dc conductivity deviated from the linearity at temperature less than 350 K (above which the SPH law is valid). Therefore, we attempted to apply the variable-range hopping (VRH) models [28,49] to the present glass as reported for V_2O_5–NiO–TeO_2 [58] and V_2O_5–BaO–B_2O_3 [27] glasses. However, the validity of such a high temperature range is not beyond question. But it has been pointed out that depending on the strength of coulomb interaction the expression for the density of states at the Fermi level is modified and the VRH [28,49] may be applied even at high temperatures ~300 K and above, though the VRH should actually be applicable in the low temperature regime (below $\theta_D/4$), normally below 100 K. For this glass we, therefore, attempted to apply the VRH model proposed by Greave's [29] which is valid for the intermediate range of temperature.

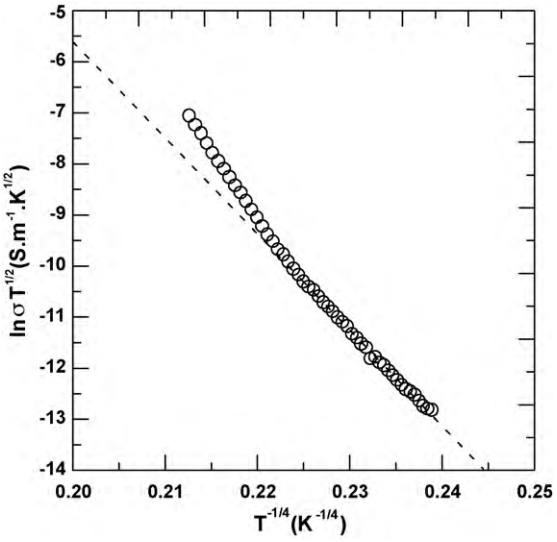

Fig. 14. Direct current electrical conductivity as a function of reciprocal temperature according to Eq. (21), of the as-quenched glass of the compositions 31.4 Bi_2O_3–2.33 Pb_3O_4–64.53 CuO–1.74 K_2O in mol%.

In the investigated temperature range (below $\theta_D/2$), no $\ln\sigma \sim T^{-1/4}$ dependence for VRH, proposed by Mott [28] has been observed. However, the procedure suggested by Greave's [29] as a modification of Mott's model of VRH [28] could be applied at intermediate temperature (below $\theta_D/2$) and proposed the following expression for the dc conductivity:

$$\sigma T^{1/2} = A \exp\left(\frac{-B}{T^{1/4}} \right) \quad (21)$$

where A and B are constants and B is given by

$$B = 2.1 \left[\frac{\alpha^3}{kN(E_F)} \right]^{1/4} \quad (22)$$

Fig. 14 shows the relationship $\log(\sigma T^{1/2})$ against $T^{-1/4}$ drawn by rearranging the data from Fig. 13. A good fit to the experimental data to expression (21) in the intermediate temperature range (295–350 K), suggesting that Greave's VRH may be valid in this glass over the entire temperature range. The values of parameters A and B obtained from this curve are given in Table 3. Using the slope obtained from this linear relation and the value of $N(E_F)$ given in Table 3 we can apply expression (22) to calculate the factor α. These values of α and $N(E_F)$ are reasonable for the localized states and consistent with those of the usual semiconducting oxide glasses [26,30]. Also, this VRH model is found suitable to explain the intermediate temperature (below $\theta_D/2$) conductivity data of this glass. Thus we conclude that appearance of the intermediate VRH at $T = 295$–350 K is reasonable for the present glass [26,30].

4. Conclusion

The present work is an extension to our previous inspection concerning the observation of ferroelectricity in a single phase glass [12–14]. Glass sample of the composition 31.4 Bi_2O_3–2.33 Pb_3O_4–64.53 CuO–1.74 K_2O in mol% was prepared by the conventional quenching melt technique. X-ray diffraction and transmission electron microscopy as well as differential thermal analysis were used to recognize the glassy nature of the as-quenched sample. Ac dielectric measurements were performed at

different applied frequencies as a function of temperature. The as-quenched glass shows attractive ferroelectric properties which is not familiar in the field of glass science. If the as-quenched glass is heat treated at or above the glass transition temperature all signs of ferroelectricity disappears completely. Furthermore, non-linear behavior of the polarization as a function of applied electric field and temperature was studied. In addition pyroelectric property was monitored and studied. On the other hand the dc electrical conductivity of the present glass can be fitted with Mott's model of nearest neighbor hopping at high temperature, while at intermediate temperature the Greaves VRH (variable-range hopping) model was found to be appropriate. The conduction was confirmed to obey the adiabatic small polaron hopping (SPH) and was mainly due to electronic transport between Cu ions. The dominant factor determining conductivity was the hopping carrier mobility in this glass. From the best fits, reasonable values of various SPH and VRH parameters are obtained.

References

[1] W. Klement, R.H. Willens, P. Duwez, Nature 187 (1960) 869–870.
[2] A.A. Bahgat, E.E. Shaisha, J. Non-Cryst. Solids 56 (1983) 243.
[3] M. Eibschutz, M.E. Lines, Hyperfine Interact. 27 (1986) 47.
[4] Robert H. Doremus, Glass Science, 2nd ed., John Wiley & Sons, Inc., New York, 1994.
[5] M.E. Lines, Phys. Rev. B 15 (1977) 388.
[6] M.E. Lines, Phys. Rev. B 17 (1978) 1984.
[7] A.M. Glass, M.E. Lines, K. Nassau, J.W. Shiever, Appl. Phys. Lett. 31 (1977) 249.
[8] H. Zhang, M. Widom, J. Magn. Magn. Mater. 122 (1993) 119.
[9] H. Zhang, M. Widom, Phys. Rev. B 51 (1995) 8951.
[10] G. Ayton, M.J.P. Gingras, G.N. Patey, Phys. Rev. Lett. 75 (1995) 2360.
[11] G. Ayton, M.J.P. Gingras, G.N. Patey, Phys. Rev. E 56 (1997) 562.
[12] A.A. Bahgat, T.M. Kamel, Phys. Rev. B 63 (2001), 012101.
[13] A.A. Bahgat, T.M. Kamel, Ferroelectrics 271 (2002) 39.
[14] A.A. Bahgat, Phys. Status Solidi A 200 (2003) R1–R4.
[15] S. Alexander, Phys. Rep. 296 (1998) 65.
[16] S. Mukherjee, B.K. Chaudhuri, H. Sakata, Phys. Rev. B 68 (2003), 016101.
[17] S. Mukherjee, B.K. Chaudhuri, H. Sakata, Phys. Rev. B68 (2003), 229901E.
[18] S. Mukherjee, H. Sakata, B.K. Chaudhuri, S. Mollah, H.D. Yang, J. Appl. Phys. 94 (2) (2003) 1211.
[19] S.A. Gridnev, N.I. Repnikov, Phys. Status Solidi B 243 (1) (2006) R4–R6.
[20] S.A. Geridnev, N.I. Repnikov, Phys. Solid State (FTT) 48 (6) (2006) 1163.
[21] S. Bhattacharya, D.K. Modak, P.K. Pal, B.K. Chaudhuri, Mater. Chem. Phys. 68 (2001) 239.
[22] A.A. Bahgat, S.A. Eissa, S.H. Salah, J. Mater. Sci. Lett. 13 (1994) 826; A.A. Bahgat, S.A. Eissa, A.I. Sabry, S.H. Salah, E.E. Shaisha, I.I. Shaltout, J. Mater. Sci. 30 (1995) 5644.
[23] V. Lyahovitskaya a, I. Zon, Y. Feldman, S. Cohen, A.K. Tagantsev, I. Lubomirsky, Adv. Mater. 15 (21) (2003) 1826.
[24] V. Lyahovitskaya, I. Zon, Y. Feldman, S. Cohen, I. Lubomirsky, Mater. Sci. Eng. B 109 (2004) 167–169.
[25] W. Ma, L. Eric Cross, Appl. Phys. Lett. 79 (26) (2001) 4420.
[26] M.M. El-Desoky, H.S.S. Zayed, F.A. Ibrahim, H.S. Ragab, Physica B 404 (2009) 4125.
[27] M.M. El-Desoky, Phys. Status Solidi A 195 (2) (2003) 422.
[28] N.F. Mott, J. Non-Cryst. Solids 1 (1968) 1.
[29] G.N. Greaves, J. Non-Crsyt. Solids 11 (1973) 427.
[30] M.M. El-Desoky, J. Non-Cryst. Solids 351 (2005) 3139.
[31] H. Mori, K. Gotoh, H. Sakata, J. Non-Cryst. Solids 183 (1995) 122.
[32] I.G. Austin, N.F. Mott, Adv. Phys. 18 (1969) 41.
[33] H.H. Qiu, H. Sakata, T. Hirayama, Ceram. Soc. Jpn. 104 (1996) 1004.
[34] I. Ardelean, H.H. Qiu, H. Sakata, Mater. Lett. 32 (1997) 335.
[35] T. Holstein, Ann. Phys. 8 (1959) 343.
[36] V.N. Bogomolov, E.K. Kudinev, U.N. Firsov, Sov. Phys. Solid State 9 (1968) 2502.
[37] M.S. Al-Assiri, M.M. El-Desoky, A. Al-Hajry, A. Al-Shahrani, A.M. Al-Mogeeth, A.A. Bahgat, Physica B 404 (2009) 1437.
[38] A.A. Bahgat, Mater. Sci. Eng. B 26 (1994) 103.
[39] A.A. Bahgat, E.A. Mahmoud, A.S. Abd Rabo, I.A. Mahdy, Physica B 382 (2006) 271–278.
[40] B.H. Venkataraman, K.B.R. Varma, Ferroelectrics Lett. 33 (2006) 39–56.
[41] D. Viehland, S.J. Jang, L. Eric Crossa, J. Appl. Phys. 69 (9) (1991) 6595.
[42] M.E. Lines, A.M. Glass, Principles and Applications of Ferroelectrics and Related Materials, Clarendon press, Oxford, 1977.
[43] A.A. Bahgat, J. Non-Cryst. Solids 226 (1998) 155–161.
[44] C. Kittel, Introduction to Solid State Physics, 4th ed., John Wiley & Sons, Inc., New York, 1971, p. 465.
[45] S.B. Lang, Phys. Today 58 (8) (2005) 31.
[46] C.F. Drake, I.F. Scanlan, United States Patent 3,850,603 (1974).
[47] A. Miller, E. Abrahams, Phys. Rev. 120 (1960) 745.
[48] A. Ghosh, B.K. Chaudhuri, J. Non-Cryst. Solids 83 (1986) 151.
[49] L. Friedman, T. Holestein, Ann. Phys. 21 (1963) 494.
[50] D. Emin, T. Holstein, Ann. Phys. (NY) 53 (1969) 439.
[51] M.B. Field, J. Appl. Phys. 40 (1969) 2628.
[52] H. Nasu, K. Hirao, N. Soga, J. Am. Ceram. Soc. 64 (1981) C63.
[53] N.F. Mott, Adv. Phys. 16 (1967) 49.
[54] S. Chakrabaty, M. Sadhukhan, D.K. Modak, B.K. Chaudhuri, J. Mater. Sci. 30 (1995) 5139.
[55] M.M. El-Desoky, N.M. Tashtoush, M.H. Habib, J. Mater. Sci.: Mater. Electron. 16 (2005) 533.
[56] N.F. Mott, E.A. Davis, Electronic Processes in Non-Crystalline Materials, Clarendon, Oxford, 1979.
[57] M.H. Cohen, J. Non-Crsyt. Solids 4 (1979) 391.
[58] C.H. Chung, J.D. Mackenzie, J. Non-Cryst. Solids 42 (1980) 357.
[59] M.M. El-Desoky, J. Mater. Sci.: Mater. Electron. 14 (2003) 215.